

Microwave Sensor Using Metamaterials

Ming Huang¹ and Jingjing Yang²
*School of Information Science and Engineering,
Yunnan University, Kunming, Yunnan 650091
PR China*

1. Introduction

It is well known that electromagnetic wave can be applied to wireless communication, radar, heating and power transmission. It has brought human society into industrial and information age. The mechanism behind these applications is electromagnetic radiation, i.e. energy transportation and conversion. Recently, research shows that evanescent wave, which is non-radiation wave associated with guided wave theory, can be amplified by metamaterials. Moreover, the sensitivity and resolution of sensor using metamaterials can be dramatically enhanced. The metamaterial-assisted sensors hope to fuel the revolution of sensing technology.

This chapter aims at the study of metamaterial-assisted sensors. Firstly, traditional microwave sensors are concisely reviewed, with emphasis on the method of microwave coupling, and the working principle of resonant microwave sensor. Then, the properties of metamaterials and its application are introduced. Enhancement of sensitivity in slab waveguide with TM mode and subwavelength resolution properties of perfect slab lens are demonstrated. The mechanisms of metamaterials for amplifying evanescent wave and for improving sensitivity and resolution are studied. Thirdly, the simulation results of the microwave sensor using epsilon near-zero materials (ENZ) and metamaterial particles are given. At last, the metamaterial-assisted open resonators are discussed.

2. Microwave sensor

Different from the famous radar and remote sensing technology, microwave sensor can measure properties of materials based on microwave interaction with matter, and it can be used to provide information about the moisture content, density, structure and shape of materials, and even chemical reaction. Microwave sensor offers many advantages over traditional sensor such as rapid measurement, nondestructive, precise, fully automated and it can be made in a laboratory or on-line. General speaking, there are two kinds of microwave sensor, i.e., nonresonant and resonant. A decided advantage of resonant sensor compared with the nonresonant sensor is that resonant sensor have higher sensitivity, simpler signal processing, and lower cost (Kupfer, 2000; Huang et al, 2007).

One of the key issues related to microwave sensor is the technique of coupling microwave to test materials. Dozens of techniques have been proposed in the past (Von Hippel, 1995). Generally, there are eight categories coupling mechanisms for microwave sensor as shown

in Fig. 1, i.e., transmission-aperiodic-closed (TAC), reflection-aperiodic-closed (RAC), transmission-aperiodic-open (TAO), reflection-aperiodic-open (RAO), transmission-resonant-closed (TRC), reflection-resonant-closed (RRC), transmission-resonant-open (TRO), and reflection-resonant-open (RRO) (Kraszewski, 1991). The schematic diagram of TRC sensor is shown in Fig. 2. It consists of a resonant cavity, a microwave generator, an interface circuit, a detecting circuit and a computer. The computer is in charge of signal processing. The detecting circuit is composed of a linear detector, a low-pass filter and a high speed A/D converter. Measurement principle is the microwave cavity perturbation techniques. Let Q_0 and f_0 be the quality factor and resonance frequency of the cavity in the unperturbed condition, respectively, and Q and f the corresponding parameters of the cavity loaded with sample. When a small sample is introduced in a cavity, it causes a frequency shift $\Delta\omega$, and the Q factor is changed accordingly. These quantities are given by (Huang et al, 2007):

$$\Delta\omega/\omega = -\omega_0(\epsilon_r' - 1) \int_{V_e} E_0^* \cdot E dv / 4W \tag{1}$$

$$1/Q - 1/Q_0 = 2\epsilon_0\epsilon_r'' \int_{V_e} E_0^* \cdot E dv / 4W \tag{2}$$

where $W = \int_{V_e} [(E_0^* \cdot D_0 + H_0^* \cdot B_0) + (E_0^* \cdot D_1 + H_0^* \cdot B_1)] dv$, $\Delta\omega = f - f_0$, $f_0 = \omega_0/2\pi$, E_0^* , D_0 , B_0 and H_0 are the fields in the unperturbed cavity, D_1 and H_1 are the fields in the interior of the sample. V_c and V_e are the volumes of the cavity and the sample respectively, dv is the elemental volume. Obviously, the measurement of Q factor and resonant frequency is a key issue for TRC sensor, and the larger the Q factor of the cavity the higher the sensitivity.

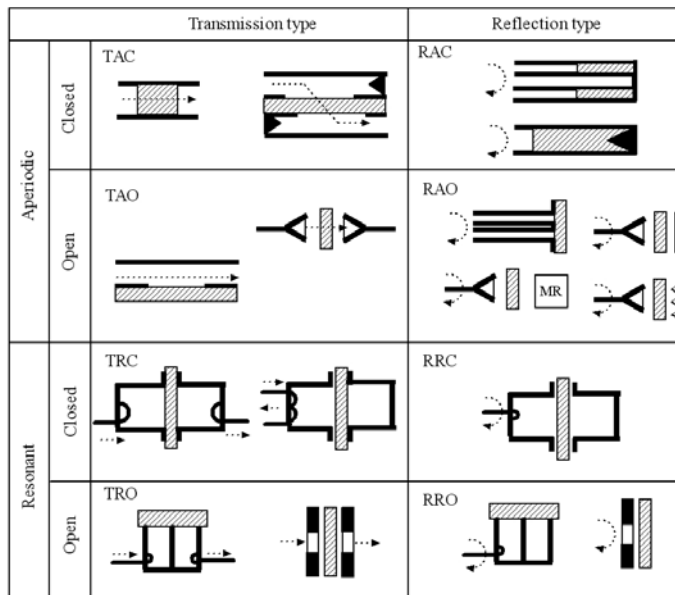


Fig. 1. Classification of eight generic types of microwave sensors for monitoring properties of industrial materials (Kraszewski, 1991)

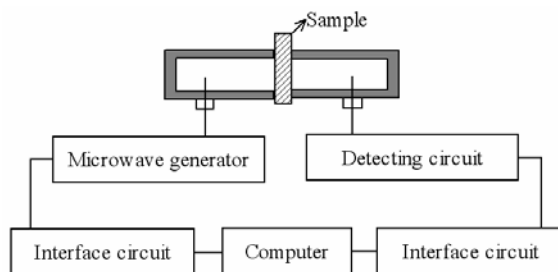


Fig. 2. The schematic diagram of the microwave sensor

3. Metamaterials

3.1 Overview of metamaterials and its sensing applications

In the 1960s, Russian theoretical physicist Veselago realized that if materials could be properly engineered, their index of refraction could be negative (Veselago, 1968). Veselago's work implied that flat materials with simultaneously negative values of permittivity and permeability could act like lenses and produce other counterintuitive phenomena, such as a reverse Dopple effect and negative refraction. It took more than 30 years, but in 2001, researchers led by Pendry, a theoretical physicist at Imperial College London, and Smith, now at Duke University, made just such a material (Shelby et al, 2001). Since then, electromagnetic metamaterials, which is artificial materials, whose permittivity and/or permeability can be designed to continuously change from negative to positive values, attract great attention all over the world. Many novel applications are proposed based on metamaterials, such as cloak, concentrators, directive antenna, superscatterers, superabsorbers, transparent devices and so on. Now, physicists and materials scientists realize that the losses is a big problem for practical applications of metamaterials (Service, 2010).

However, the properties of metamaterials, usually regarded as detrimental, are either of no importance for sensor application or may even enhance it. For instance, the sharp resonant peaks in dispersion are convenient since they may mean an increased sensitivity of sensor and actually the sharper the peaks are, the better. Since the sensor can be made to operate at a single frequency, there is no need for broadband materials. One of the unavoidable drawbacks of the metamaterials, large absorption losses, is practically of no importance here (Zoran et al, 2007). Moreover, due to evanescent waves can be amplified by metamaterials, the sensor using metamaterials possesses the characteristics of sub-wavelength resolution (Pendry, 2000) and high sensitivity. Since sensitivity and resolution are two vital parameters of sensor, metamaterials will open up an avenue for improving the performance of sensors. The first revolutionary products using metamaterials might be the metamaterial-assisted sensors.

3.2 Enhancement of sensitivity in slab waveguide

Fig. 3 shows the model of integrated slab waveguide. In the case of time harmonic field and lossless, i.e., both ϵ and μ are all real numbers, suppose that magnetic field H is polarized along the y -axis, TM wave travels in the z -direction, and $H_y = H_y(x)e^{j(\omega t - \beta z)}$, then wave equation is simplified into the following well-known scalar Helmholtz equation:

$$\partial^2 H_y(x) / \partial z^2 + (\omega^2 \varepsilon(x) \mu(x) - \beta^2) H_y(x) = 0 \quad (3)$$

and

$$E_z(x) = (1/j\omega\varepsilon(x))(\partial H_y(x) / \partial x). \quad (4)$$

where ω is angular frequency of the field and β is the propagation constant in z-direction, which can be written as $\beta = k_0 N$, where k_0 is the free space wave number and N is the modal effective index. The structure of the model is illustrated as followings: in the non working region, a guiding layer is sandwiched between semi-infinite cladding and substrate, where d_1 is the thickness of the guiding layer, ε_c and μ_c , ε_g and μ_g , ε_s and μ_s are the permittivity and permeability of the cladding, guiding and substrate layer, respectively. In the working region, there is a layer of metamaterials with negative permittivity ε_m , negative permeability μ_m , and thickness d_2 .

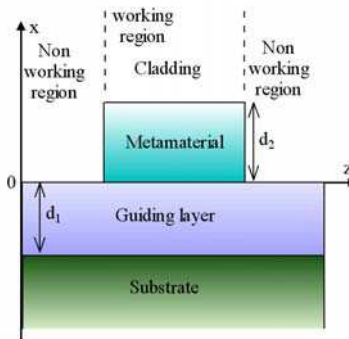


Fig. 3. Schematic structure of integrated slab waveguide sensor with a metamaterial layer
In the working region, the solution forms of Eq. (3) in each layer are shown as followings:

$$H_{yc}(x) = A e^{-\gamma_c(x-d_2)} e^{-j\beta z}, \quad x > d_2, \quad (5)$$

$$H_{ym}(x) = (B_1 e^{-\gamma_m x} + B_2 e^{\gamma_m x}) e^{-j\beta z}, \quad 0 < x < d_2, \quad (6)$$

$$H_{yg}(x) = (D_1 \cos(\gamma_g x) + D_2 \sin(\gamma_g x)) e^{-j\beta z}, \quad -d_1 < x < 0, \quad (7)$$

$$H_{ys}(x) = F e^{\gamma_s(x+d_1)} e^{-j\beta z}, \quad x < -d_1, \quad (8)$$

where $\gamma_c = \sqrt{\beta^2 - \varepsilon_0 \varepsilon_c \mu_c \omega^2}$, $\gamma_m = \sqrt{\beta^2 - \varepsilon_0 \varepsilon_m \mu_m \omega^2}$, $\gamma_g = \sqrt{\varepsilon_0 \varepsilon_g \mu_g \omega^2 - \beta^2}$ and

$\gamma_s = \sqrt{\beta^2 - \varepsilon_0 \varepsilon_s \mu_s \omega^2}$, respectively. Constants A , B_1 , B_2 , D_1 , D_2 and F represent the amplitude of the waves in each layer, and need to be determined from the boundary conditions that require H_y and E_z to be continuous at $x = -d_1$, 0 , and d_2 , respectively. Substituting Eqs. (5)-(8) into Eq. (4), we get E_z for each layer, and also the boundary conditions and the corresponding constants as follows:

$$\tan(\gamma_g d_1) = (\gamma_g \epsilon_g D_1 - \gamma_g \epsilon_g D_2) / (\gamma_g \epsilon_g D_1 + \gamma_g \epsilon_g D_2) \tag{9}$$

$$B_1 = 0.5(D_1 - \gamma_g \epsilon_m D_2 / \gamma_m \epsilon_g), B_2 = 0.5(D_1 + \gamma_g \epsilon_m D_2 / \gamma_m \epsilon_g), \tag{10}$$

$$B_1 = 0.5(1 + \gamma_c \epsilon_m / \gamma_m \epsilon_c) e^{\gamma_m d_2} A, \tag{11}$$

$$B_2 = 0.5(1 - \gamma_c \epsilon_m / \gamma_m \epsilon_c) e^{-\gamma_m d_2} A, \tag{12}$$

After some algebraic manipulations the dispersion equation of the working region can be written as:

$$\gamma_g d_1 = \arctan \left(\frac{\gamma_m \epsilon_g}{\gamma_g \epsilon_m} \left(\frac{(\gamma_m \epsilon_c + \gamma_c \epsilon_m) - (\gamma_m \epsilon_c - \gamma_c \epsilon_m) e^{-2\gamma_m d_2}}{(\gamma_m \epsilon_c + \gamma_c \epsilon_m) + (\gamma_m \epsilon_c - \gamma_c \epsilon_m) e^{-2\gamma_m d_2}} \right) \right) + \arctan \left(\frac{\gamma_s \epsilon_g}{\gamma_g \epsilon_s} \right) + m\pi, \tag{13}$$

where $m=0, 1, 2, \dots$ is the mode order. When d_2 approaches zero, i.e., no metamaterial is available, Eq. (13) is reduced to the well-known dispersion equation for a three-layer slab linear waveguide given by

$$\gamma_g d_1 = \arctan \left(\frac{\gamma_s \epsilon_g}{\gamma_g \epsilon_s} \right) + \arctan \left(\frac{\gamma_c \epsilon_g}{\gamma_g \epsilon_c} \right) + m\pi. \tag{14}$$

When $\gamma_c \epsilon_m = -\gamma_m \epsilon_c$, according to Eqs. (6), (7), (11) and (12), we get $B_1=0$, and $A = D_1 e^{\gamma_m d_2}$. Compared with that in the nonworking region, where $A = D_1$, the amplitude of evanescent wave is enhanced by $e^{\gamma_m d_2}$ due to the existence of metamaterial layer. Eq. (13) can be reduced to Eq. (14). Therefore, the same dispersion equation holds for both the working region and the nonworking region, and consequently the propagation constants for the two regions are identical.

Fig. 4 shows the distribution of magnetic field $H_y(x)$. It can be seen that the evanescent wave in cladding layer is enhanced by metamaterials. It indicates that metamaterials could be used to amplify the evanescent wave in the cladding layer without affecting the propagation constant of the waveguide.

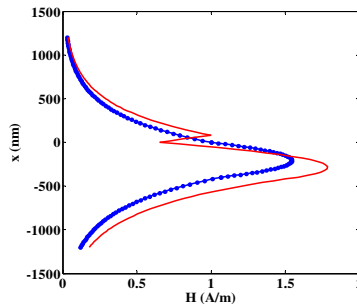


Fig. 4. Magnetic field $H_y(x)$ distribution in three-layer waveguide conventional sensor (blue dot line) and the proposed sensor with metamaterials (red line), d_2 is the thickness of the metamaterials

For the sake of simplicity in the evaluation of the sensitivity, it is assumed that $\gamma_c = k_0 q_c$, $\gamma_m = k_0 q_m$, $\gamma_g = k_0 q_g$ and $\gamma_s = k_0 q_s$, where $q_c = \sqrt{N^2 - \epsilon_c}$, $q_m = \sqrt{N^2 - n\epsilon_m}$, and n is a negative number, $q_g = \sqrt{\epsilon_g - N^2}$ and $q_s = \sqrt{N^2 - \epsilon_s}$. The sensitivity of the proposed waveguide sensor is obtained in a condensed form, three normalized effective indices X_s , X_c and X_m and three asymmetry parameters a_s , a_c and a_m are defined as $X_s = q_s/q_g$, $X_c = q_c/q_g$, $X_m = q_m/q_g$, $a_s = \epsilon_s/\epsilon_g$, $a_c = \epsilon_c/\epsilon_g$, and $a_m = \epsilon_m/\epsilon_g$. In the light of these assumptions, Eq. (13) can be written as

$$k_0 q_g d_1 = \arctan(X_s/a_s) + \arctan(X_m b_1/(a_m b_2)) + m\pi. \quad (15)$$

where $b_1 = (a_c X_m + a_m X_c) - (a_c X_m - a_m X_c) e^{-2k_0 X_m q_g d_2}$ and

$$b_2 = (a_c X_m + a_m X_c) + (a_c X_m - a_m X_c) e^{-2k_0 X_m q_g d_2}.$$

In the case of homogenous sensing, the sensitivity S is defined as the ratio of the modal effective index N change of the guided mode to the refractive index change of the cover n_c . The sensitivity $S_2 = (\partial N / \partial n_c)$ is calculated by differentiating Eq. (15) with respect to N and n_c .

After some algebraic manipulations, the sensitivity of proposed sensor can be written as

$$S_2 = \frac{\sqrt{a_c q} X_m \left[\left(2 \frac{X_m}{\epsilon_g} q_g^2 + \frac{a_m}{X_c} \right) e^{-f} (b_1 + b_2) - \left(2 \frac{X_m}{\epsilon_g} q_g^2 - \frac{a_m}{X_c} \right) (b_2 - b_1) \right]}{\left(A_{\text{mTM}} + \frac{a_s (1 + X_s^2)}{X_s (a_s^2 + X_s^2)} \right) \left(\frac{a_m^2 b_2^2 + X_m^2 b_1^2}{a_m} \right) + b_1 b_2 \frac{C_1}{X_m} + G_1 + G_2}, \quad (16)$$

where $f = 2k_0 X_m q_g d_2$, $G_1 = (b_2 - b_1)(a_c C_1 + a_m X_m C_2 / X_c)$,

$$G_2 = e^{-f} (b_2 + b_1) ((a_c X_m - a_m X_c) f / X_m - a_c C_1 + C_2 a_m X_m / X_c),$$

$A_{\text{mTM}} = \arctan(X_s/a_s) + \arctan(X_m b_1/(a_m b_2)) + m\pi$, $C_1 = 1 + X_m^2$, and $C_2 = 1 + X_c^2$.

In a similar manner, Eq. (14) is differentiated to obtain the sensitivity S_1 of the three-layer waveguide conventional sensor without metamaterials. As a result, it can be obtained that

$$S_1 = \frac{2 / \sqrt{a_c q} - \sqrt{a_c q}}{1 + X_c^2 + rF}. \quad (17)$$

where $q = (1 + X_s^2)/(a_s + X_s^2)$, $r = X_c(a_c^2 + X_c^2)/a_c$,

$F = \arctan(X_s/a_s) + \arctan(X_c/a_c) + m\pi + a_s(1 + X_s^2)/(X_s(a_s^2 + X_s^2))$. The variation curves of sensitivity S_2 with the different values of thickness d_2 are shown in Figs. 5. It can be noted that sensitivity goes up with the increasing thickness d_2 of the metamaterials. This is a unique property of metamaterials. It indicates that sensitivity can be enhanced by increasing the thickness of metamaterial layer.

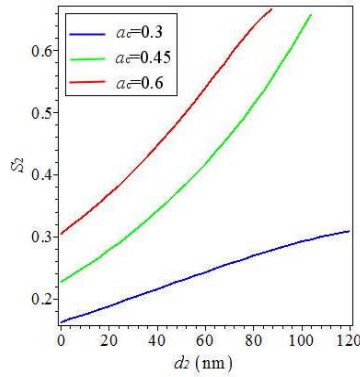


Fig. 5. Sensitivity S_2 versus the thickness of the metamaterials d_2 for different values of a_c , $a_s=0.62$, $a_m=-0.5$, $n=-0.6$, and $d_1=400\text{nm}$

We have verified that the metamaterials can amplify evanescent waves, and the sensitivity of sensors with TM mode can be dramatically enhanced compared with the conventional three-layer TM wave waveguide sensor without metamaterials. The other works about slab waveguide sensor can also be found in the work of Qing and Taya et al (Qing et al, 2004; Taya et al, 2009) However, to the best of our knowledge, there is no report about experimental results till now.

3.2 Enhancement of resolution based on metamaterials

Assume TE wave transmitting along z-axis in Fig. 6, when $\omega^2 c^{-2} > k_x^2 + k_y^2$, $k_z = \sqrt{\omega^2 c^{-2} - k_x^2 - k_y^2} \approx \omega c^{-1} = \beta = 2\pi/\lambda$, the electric field of radiation wave is defined as $E^i = E_y^i e^{-j(\omega t - \beta z)}$. Its transmission properties on the interface between two dielectrics can be obtained according to the equation of plane wave (Guru & Hizioglu, 1998).

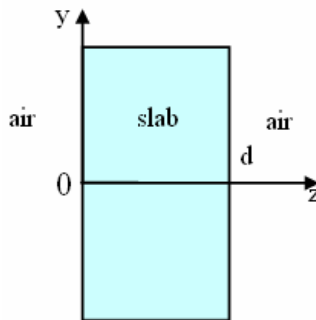


Fig. 6. Model of the metamaterial slab

When $\omega^2 c^{-2} < k_x^2 + k_y^2$, the electric field of evanescent wave is given by $E^i = E_y^i e^{j(k_z z + k_x x - \omega t)}$, where the wave vector $k_z = j\sqrt{k_x^2 + k_y^2 - \omega^2 c^{-2}}$, implies exponential decay. The reflected and

transmitted wave are $E^r = E_y^r e^{j(-k_z z + k_x x - \omega t)}$, $E^t = E_y^t e^{j(k'_z z + k_x x - \omega t)}$, where $k'_z = j\sqrt{k_x^2 + k_y^2 - \epsilon\mu\omega^2 c^{-2}}$, the corresponding magnetic field H_x can be obtained according to $\nabla \times \vec{E} = -\partial \vec{B} / \partial t$, and $H_x = 1/j\omega\mu\mu_0 (\partial E_y / \partial z)$. By matching boundary condition of E_y and H_x at $z=0$, we can obtain the following equations $E_y^i + E_y^r = E_y^t$, $(k_z/\omega\mu_0)E_y^i - (k_z/\omega\mu_0)E_y^r = (k'_z/\omega\mu\mu_0)E_y^t$. After some algebraic manipulations the coefficient of transmission and reflection can be written as

$$t = E_y^t / E_y^i = 2\mu k_z / (\mu k_z + k'_z) \text{ and } r = E_y^r / E_y^i = (\mu k_z - k'_z) / (\mu k_z + k'_z). \tag{18}$$

Conversely a wave inside the medium incident on the interface with vacuum experiences transmission and reflection as follows:

$$t' = 2k'_z / (k'_z + \mu k_z) \text{ and } r' = (k'_z - \mu k_z) / (k'_z + \mu k_z). \tag{19}$$

To calculate transmission through both surfaces of the slab we must sum the multiple scattering events,

$$T = tt'e^{jk'_z d} + tt'r'^2 e^{3jk'_z d} + tt'r'^4 e^{5jk'_z d} + \dots = tt'e^{jk'_z d} / (1 - r'^2 e^{2jk'_z d}) \tag{20}$$

By substituting from (19) and (20) and taking the limit,

$$\lim_{\substack{\mu \rightarrow -1 \\ \epsilon \rightarrow -1}} T = e^{-jk'_z d} = e^{-jk_z d} \tag{21}$$

The reflection coefficient is given by

$$\lim_{\substack{\mu \rightarrow -1 \\ \epsilon \rightarrow -1}} R = 0 \tag{22}$$

The Eqs.(21) and (22) was firstly derived by Pendry (Pendry, 2000). It indicates that both propagating wave and evanescent wave contribute to the resolution of the image. Therefore, there is no physical obstacle to perfect reconstruction of the image beyond practical limitations of apertures and perfection of the lens surface.

Based on the method of transformation optics, the performance of perfect slab lens can be simulated. The coordinate transformation between transformed space and the original space of the perfect slab lens is shown as follows (Wang et al, 2008).

$$x = \begin{cases} x' + b & x' < 0 \\ \delta x' + b & 0 \leq x' < b, y = y', z = z' \\ x' + \delta b & x' > b \end{cases} \tag{23}$$

The corresponding material parameters are

$$\epsilon_{x'} = \mu_{x'} = 1/\delta, \epsilon_{y'} = \mu_{y'} = \delta, \epsilon_{z'} = \mu_{z'} = \delta \tag{24}$$

where δ is a small number with positive value and the perfect slab lens can be obtained as δ goes to zero. Simulation results of the slab lens are shown in Fig. 7. From Fig.7 (a) and (b), it is seen that the propagating wave as well as the evanescent wave, are directionally guided

along x-axis to the right side by the slab lens, and the object totally duplicated to the image plane. The same phenomenon can be observed when reduce the size of the object or diminish the thickness of the slab, as shown in Fig. 7(c) and (d). The image of the object can be enlarged with proper coordinate transmission.

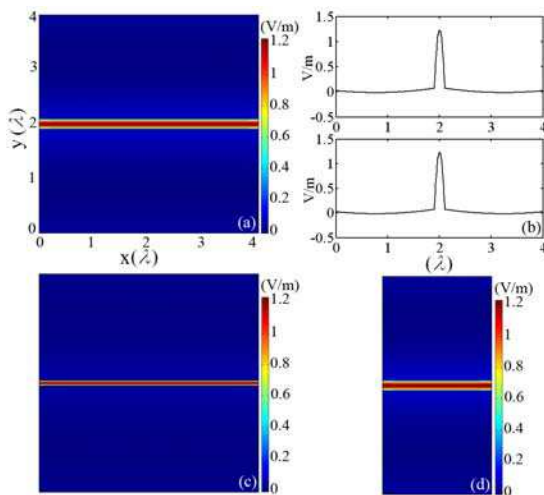


Fig. 7. Electric field (E_z) distribution in the planar perfect lens. (a) The thickness of the slab is $b = 4\lambda$, the size of the object is $t = 0.2\lambda$. (b) Electric field distribution on the object (up) and imaging (down) plane. (c) $b = 4\lambda$, $t = 0.1\lambda$. (d) $b = 2\lambda$, $t = 0.2\lambda$

Since the perfect lens was proposed by Pendry, imaging beyond diffraction limit have gained much attention. A series of perfect lensing structures including cylinders, spheres, corner perfect lens and superlens were developed. But the perfect resolution is difficult to realize for the inevitable losses of the realizable materials. At microwave frequency band, subwavelength detecting with resolution of 0.037λ has been realized by Shreiber et al (Shreiber et al, 2008).

4. Microwave sensor using ENZ metamaterials

The model of the microwave sensor based on ENZ metamaterials (Wu et al, 2008) is shown in Fig. 8(a). It is a 3D “dumbbell-shaped” coaxial metallic waveguide filled with ENZ metamaterials. Fig. 8(b) is a cross-sectional view, where the red region denotes the ENZ metamaterials, the grey region denotes the metallic conductor, and yellow region located at the center denotes the testing sample. The ENZ metamaterials is characterized by a Drude-type model with relative permittivity $\epsilon = 1 - \omega_p^2 / \omega(\omega + j\Gamma)$, where ω_p is the plasma frequency and Γ is the collision frequency (rad/s). In the simulations, we have taken $\omega_p R / c = \pi / 2$. Note that at $f = f_p$, the permittivity of the ENZ metamaterials is given by $\epsilon \approx j\Gamma / \omega_p \approx 0$. The incident wave is the fundamental TEM mode. The structure is uniform along the z direction. The simulation results of transmission coefficients for a variation of sample permittivity are shown in Fig. 9. It’s seen that the transmission coefficients have two

resonant peaks. The low-frequency peak is red shifted with the increase of sample permittivity, while the high-frequency peak keeps unchanged. Dielectric properties of the testing sample can be inverted by measuring the position of the low-frequency peak. When increasing the length L of the waveguide, results show that the high-frequency peak can be red shifted. It means that the high-frequency peak is mainly dependent on the Fabry-Perot resonance.

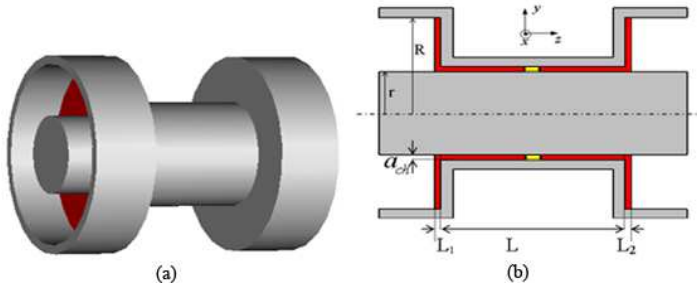


Fig. 8. (a) Model of the “dumbbell -shaped” coaxial metallic waveguide. (b) Cross-section of the model. Red region: ENZ metamaterials; Yellow region: testing sample; Grey region: metallic conductor ($R = 20mm$; $r = 8.7mm$; $L = 1.5R = 30mm$; $L_1 = L_2 = a_{ch} = R / 20 = 1mm$). [15] (Wu et al, 2008)

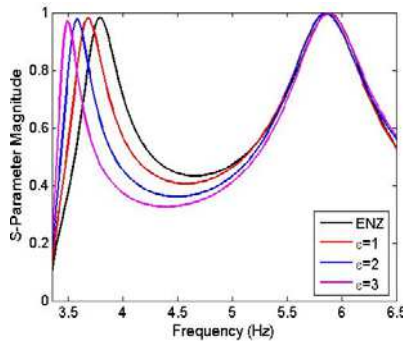


Fig. 9. Transmission coefficient for a variation of sample permittivity (Wu et al, 2008)

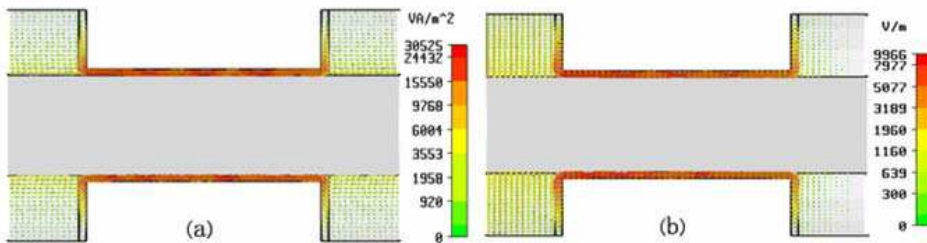


Fig. 10. The power flow distribution (a) and the electric field distribution (b) at the low-frequency transmission peak (Wu et al, 2008)

To investigate the working principle of the ENZ metamaterial-assisted microwave sensor, the power flow and the electric field distribution inside the waveguide are calculated as shown in Fig. 10. It is seen that the the power flow is squeezed through waveguide filled with ENZ metamaterials and perfectly recovered to original status at the output port. The electric field is confined into the detection zone, and as a consequence, this region will be rather sensitive to any slight change in sample permittivity.

The above simulation results show that the electromagnetic wave can be tunnelled and squeezed through 3D coaxial waveguide filled with ENZ metamaterials. The effects are similar to literature results of other guidewave structure (Silveirinha & Engheta, 2006; Alù & Engheta, 2008). The ENZ metamaterial-assisted wave guide have potential applications in microwave sensor.

5. Microwave sensor using metamaterial particles

5.1 Microwave sensor based on a single metamaterial particle

The model of the waveguide filled with a single metamaterial particle is shown in Fig. 11(a). The metamaterial particle with the thickness of 0.44mm is located at the center of the WR-14 rectangular waveguide. Since the topology structure of the particle influence the performance of the microwave sensor, the resonators with two different geometries are discussed, as shown in Fig. 11(b) and 11(c). Dimensions of the square asymmetric single split ring resonator (aSSR) are chosen as $g=1\text{mm}$, $w=0.8\text{mm}$ and $L=6.68\text{mm}$. The position of the gap is defined by the asymmetric parameter d_x . The resonator is designed onto a 0.127mm thick substrate with relative permittivity of 3. Fig. 11(c) shows the cross section of the rectangular aSSR resonator with the aspect ratio of 1/2. Its perimeter and geometric parameters are the same as the square aSSR. The black region represents dielectric sample. The simulations were conducted with the commercial software CST. Perfect electric conductor boundaries were applied to all sides of the model to simulate the waveguide. The waveguide is terminated on both sides by a waveguide port through which the electromagnetic waves enter and exit the model. The incident wave is the fundamental TE_{10} mode with electric field polarized along the y -axis and it propagates along the z -axis.

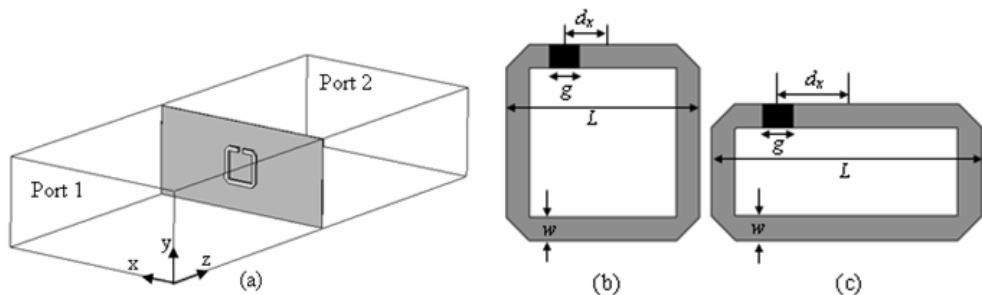


Fig. 11. (a) Simulation model of the asymmetric metamaterial particle-assisted microwave sensor. (b), and (c) show the cross section of the square aSSR and rectangular aSSR. Black region denotes the dielectric sample located in the gap (Yang et al, 2010)

The variation of Q factor as a function of asymmetric parameter is shown in Fig. 12. The position of the slit is successively moved from a close-to-symmetry position to the left resonator arm. From Fig. 12, it is seen that Q factor increases with d_x and reaches moderate

values above 1400 for the square aSSR and above 1200 for the rectangular aSSR, at $d_x = 0.9\text{mm}$ and $d_x = 1.24\text{mm}$, respectively. Therefore, the Q factor of the asymmetric metamaterial particle-assisted microwave sensor can be selected by varying the position of split or the aspect ratio of the resonator ring, which enables a high degree of design flexibility.

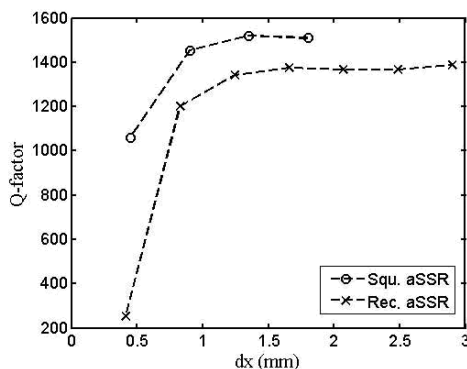


Fig. 12. The Q factor of the asymmetric metamaterial particle-assisted microwave sensor for a sweep of d_x (Yang et al, 2010)

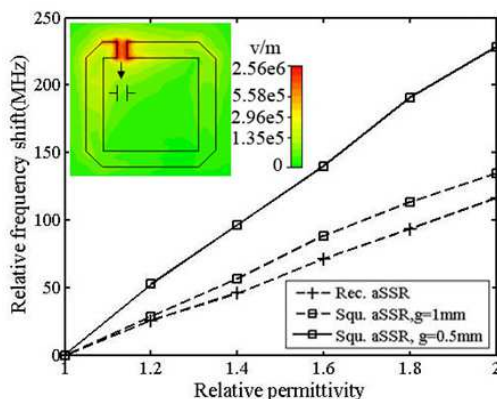


Fig. 13. Relative frequency shift of the spectral response as a function of relative permittivity of the sample located in the gap. The inset shows the normal electric field distribution for square aSSR when $g=0.5\text{mm}$, $\epsilon_r = 1$ (Yang et al, 2010)

To explore the sensitivity of the asymmetric metamaterial particle-assisted microwave sensor, dielectric material induced relative frequency shift was simulated. Results show that the peak position of transmission coefficient S_{21} is red shifted with the increase of relative permittivity of the sample located in the detecting zone. The relation between relative frequency (Δf) and sample permittivity is shown in Fig. 13. It indicates that Δf increases linearly with ϵ_r , and thus, both the square and the rectangular metamaterial resonators can be used in dielectric sensing. Dielectric properties of the testing sample can be inverted by

detecting the relative frequency shift of the output signal of the microwave sensor. Furthermore, the microwave sensor based on the square aSSR will be more accurate in dielectric sensing, since it induces a larger Δf than the rectangular aSSR for detecting the same sample. The solid line in Fig. 13 indicates that when reducing the gap size of the square aSSR to $g=0.5\text{mm}$, a much larger frequency shift can be obtained. Therefore, the sensitivity of the designed microwave sensor can be further improved by diminishing the gap size of the metamaterial resonator ring. The gap of the asymmetric metamaterial resonator ring can be modelled by a capacitor as shown in the inset of Fig.13. Diminishing the gap size g results in an enhancement of the electric field, while diminishing the distance between the left and right plates of the capacitor leads to an enhancement of the energy reservation. Field enhancement is the main reason for the improved sensitivity of the asymmetric metamaterial particle-assisted microwave sensor.

The above simulation results show that the spectral response and Q factor of the sensor can be flexibly tailed to design requirement by varying the asymmetry parameter or the topological structure of the resonator. Two resonator arms of the asymmetric structure can strongly confine the field into the gap which is very sensitive in dielectric environment. Moreover, diminishing the gap size will improve the sensitivity to a great extent. Due to the spectral response of the asymmetric metamaterial resonator can be tailed to microwave, terahertz, infrared or optical band by miniaturizing the size of the structure, the asymmetric metamaterial particle-assisted sensor will have potential applications in a wide frequency band for sensing minute amounts of dielectric sample substance.

The excitation of trapped modes by asymmetrically split rings was firstly reported by Fedotov et al.(Fedotov, et al, 2007). Then, Al-Naib et al. (Al-Naib et al, 2008) realized experimentally the thin film sensor with high Q factor by locating one unit cell of double split ring resonator in the single mode rectangular waveguide. It is believed that more experimental results about the sensors will be reported in the future.

5.2 Microwave sensor based on coupled metamaterial particles

When a waveguide is filled or partially filled with metamaterials with simultaneously negative permittivity and permeability, the transmission can be enhanced (Marqués et al, 2002). In this section, a pair of coupled metamaterial particles with Ω shape is located in the rectangular waveguide to form the microwave sensor. The simulation model is shown in Fig. 14(a). The geometric parameters for the Ω -shaped particles are chosen as $w = 0.144 \text{ mm}$, $h = 4.5 \text{ mm}$, $d = 0.1 \text{ mm}$, $R_1=1\text{mm}$ and $R_2 = 1.4 \text{ mm}$ (see Fig. 14(b)). The cross section of the rectangle waveguide is $axb=15\text{mm}\times 7.5\text{mm}$. The length is $l=12\text{mm}$. The incident wave is the fundamental TE_{10} mode propagates along the x -axis, and the incident power is 1W . The input port is at $x=0$, the output port is at $x=12\text{mm}$. Electric field and the magnetic field vectors are along the y and z -axis, respectively.

Fig. 15 shows the comparison of transmission coefficient (S_{21}) between the rectangular waveguide filled by one pair of Ω -shaped particles and the hollow waveguide. It indicates that the cutoff frequency of the hollow waveguide is 10GHz , which is in good agreement with the theoretical results ($\lambda_c = 2a$). Interestingly, the transmission coefficient of the waveguide filled with coupled metamaterial particles has two enhancement peaks at the frequency of 8.424GHz and 9.864GHz . It is worth noting that the amplitude of the transmission coefficient S_{21} is greater than 1 at the two resonant frequencies.

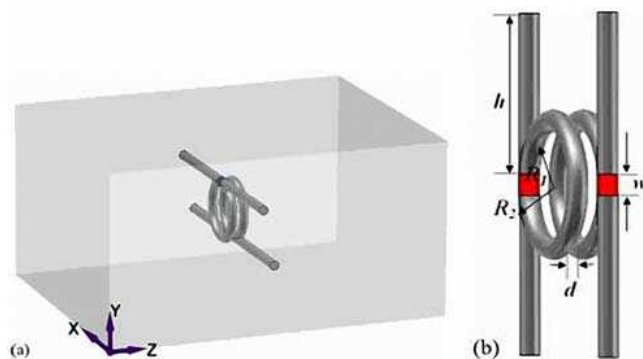


Fig. 14. (a) Perspective of the model of waveguide filled by one pair of Ω -shaped particles. (b) The Ω -shaped particles. Red region denotes the detecting zone, i.e., gap of the Ω -shaped particle (Huang et al, 2009)

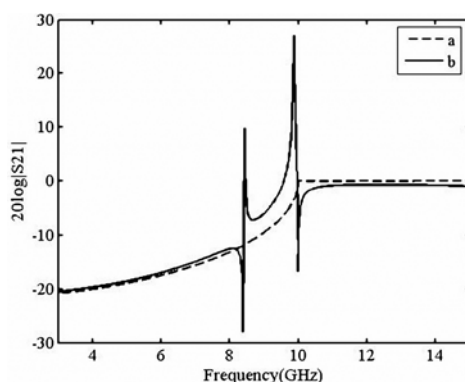


Fig. 15. Transmission coefficient (S_{21}) as a function of frequency. Line a and b denote S_{21} of hollow waveguide and the waveguide filled with coupled metamaterial particles, respectively (Huang et al, 2009)

To explore the characteristic of evanescent mode in dielectric sensing, transmission spectrum was simulated for a variation of sample permittivity, as shown in Fig. 16. It is found that in the frequency range of 7GHz to 9GHz, the evanescent mode is red shifted with the increase of permittivity, while the peak position of the cutoff mode, in the frequency range of 9.7GHz to 10.1GHz, keeps unchanged. Therefore, different dielectric materials located the detecting zone can be inverted by measuring the peak frequency of the transmission coefficient in the evanescent mode. Besides, it should be noted that the cutoff mode is dependent on the Fabry-Perot resonance, since the peak position changes with the size of waveguide. Another interesting aspect, which is visualized in Fig. 16, is the fact that the transmission responses for different dielectric are progressively shifted towards left, but their peaks are not consistent with the dielectric constant increase. The results show that the peak frequency of transmission coefficient (S_{21}) depends critically on the permittivity of the sample in the detecting zone, while the amplitude of S_{21} is a complicated function of the permittivity and topological structure of the coupled metamaterial particles.

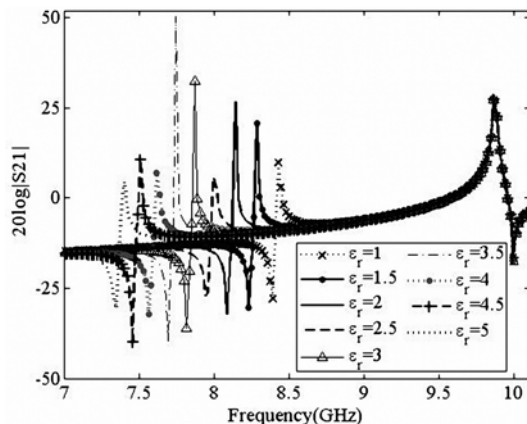


Fig. 16. Transmission coefficient (S21) versus frequency for different dielectric materials in the detecting zone (Huang et al, 2009)

To quantify the sensitivity of the evanescent mode for dielectric sensing, the performance of the metamaterial-assisted microwave sensor is compared with the traditional microwave cavity. We closed both ends of a hollow waveguide with metallic plates, which forms a conventional microwave cavity ($axbxl=15 \times 7.5 \times 12 \text{mm}^3$), and computed the resonant frequency of the cavity located with dielectric sample. Table 1 shows a comparison between the relative frequency shift, i.e., $\Delta f_N = f_N(\epsilon_1) - f_N(\epsilon_r)$ of the waveguide filled with coupled metamaterial particles, and that of the conventional microwave cavity, i.e., $\Delta f_C = f_C(\epsilon_1) - f_C(\epsilon_r)$. Where, ϵ_1 and ϵ_r denotes the relative permittivity of the air and the dielectric sample, respectively. It indicates that minimum (respectively maximum) frequency shift of the waveguide filled with Ω -shape coupled metamaterial particles is 360 times (respectively 450 times) that of the conventional microwave cavity. As a consequence, the waveguide filled with Ω -shape coupled metamaterial particles can be used as a novel microwave sensor to obtain interesting quantities, such as biological quantities, or for monitoring chemical process, etc. Sensitivity of the metamaterial-assisted microwave sensor is much higher than the conventional microwave resonant sensor.

ϵ_r	1.5	2	2.5	3	3.5	4	4.5	5
Δf_N	144	288	432	558	684	810	918	1026
Δf_C	0.4	0.7	1.1	1.3	1.6	1.8	2.2	2.5
$\Delta f_N / \Delta f_C$	360	411	393	429	428	450	417	410

Table 1. Comparison of the relative frequency shift (MHz) between the waveguide filled with coupled metamaterial particles and the conventional cavity

In addition, the microwave sensor can also be constructed by filling the other type of coupled metamaterial particles into the rectangular waveguide. For example, the meander line and split ring resonator coupled metamaterial particle (Fig. 17(a)); the metallic wire and split ring resonator (SRR) coupled metamaterial particle (Fig. 17(b)). The red regions shown in Fig. 17 denote the dielectric substances. Fig. 17(c) and (d) are the front view and the vertical view of (b).

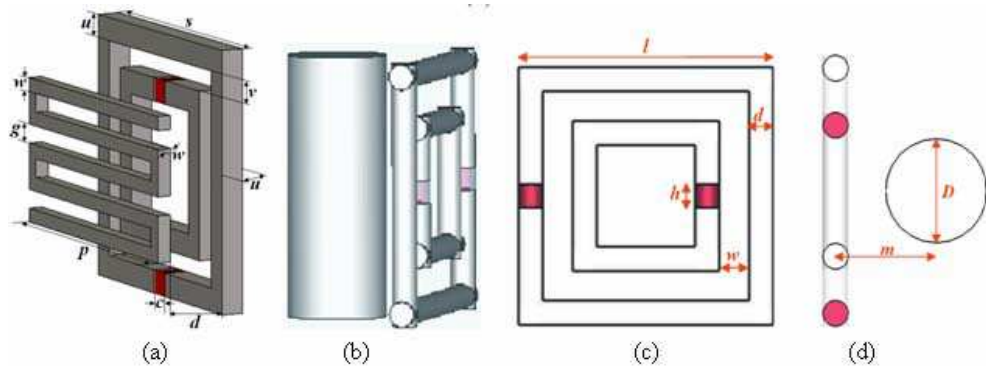


Fig. 17. (a) Configuration of the particle composed of meander line and SRR. $w = 0.15\text{mm}$, $g = 0.2\text{mm}$, $p = 2.92\text{mm}$, $d = 0.66\text{mm}$, $c = 0.25\text{mm}$, $s = 2.8\text{mm}$, $u = 0.25\text{mm}$, and $v = 0.25\text{mm}$. (b) Configuration of the particle composed of metallic wire and SRR. (c) and (d) are the front view and the vertical view of (b). $l = 1.302\text{mm}$, $h = 0.114\text{mm}$, $w = 0.15\text{mm}$, $d = 0.124\text{mm}$, $D = 0.5\text{mm}$, $m = 0.5\text{mm}$

Transmission coefficient of the waveguide filled with any of the above two couple metamaterial particles also possesses the characteristic of two resonant peaks. When it is used in dielectric sensing, electromagnetic properties of sample can be obtained by measuring the resonant frequency of the low-frequency peak, as shown in Fig. 18.

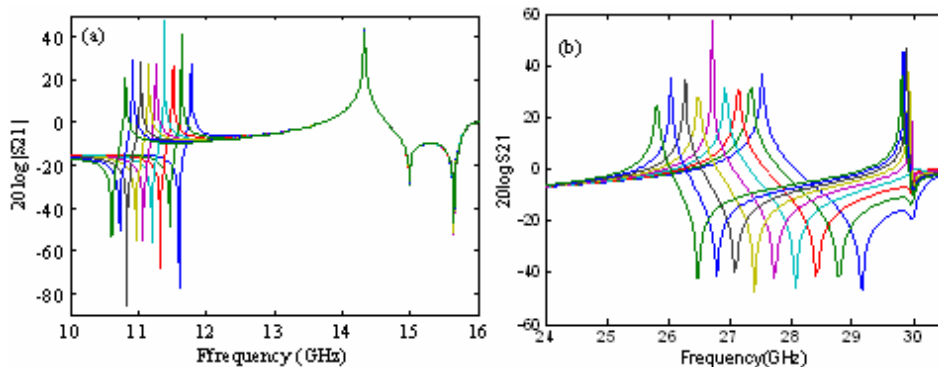


Fig. 18. Transmission coefficient ($20\log |S_{21}|$) versus frequency for a variation of sample permittivity. (a) The wave guide is filled with coupled meander line and SRR. (b) The wave guide is filled with coupled metallic wire and SRR. From right to the left, the curves are corresponding to dielectric sample with permittivity of 1, 1.5, 2, 2.5, 3, 3.5, 4, 4.5, and 5, respectively

From the above simulation results, we can conclude that the evanescent wave in the waveguide filled with coupled metamaterial particles can be amplified. The evanescent mode is red shifted with the increase of sample permittivity. Therefore, the waveguide filled with couple metamaterial particles can be used as novel microwave sensor. Compared with the conventional microwave resonant sensor, the metamaterial-assisted microwave sensor allows for much higher sensitivity.

5.3 Microwave sensor based on stacked SRRs

Simulation model of the microwave sensor based on stacked SRRs is shown in Fig. 19. The size of the waveguide is $a \times b \times L = 22.86 \times 10.16 \times 12.8 \text{ mm}$, as shown in Fig. 19(a). Fig.19(b) is the front view of the SRR with thickness of 0.03mm. It is designed onto a 0.127mm thick substrate with relative permittivity of 4.6. The geometric parameters for the SRR are chosen as $L=1.4 \text{ mm}$, $g=s=w=0.3 \text{ mm}$, $P=2 \text{ mm}$, so that the sensor works at the frequency between 8-10.5GHz. Fig. 19(c) is the layout of the stacked SRRs, the distance between two unit cell is $U=0.75$.

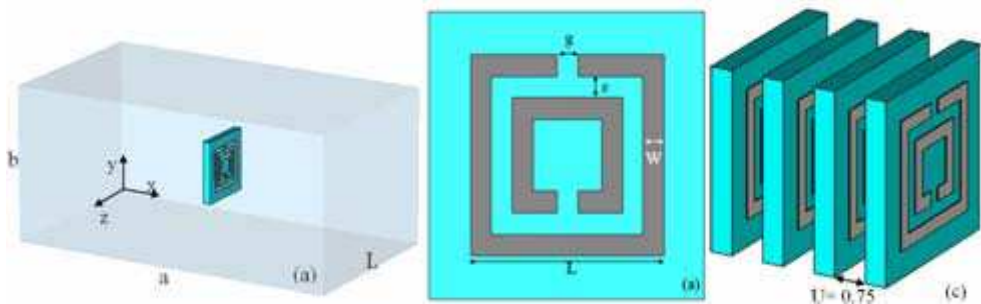


Fig. 19. (a) The microwave sensor based on stacked SRRs. (b) Front view of the SRR cell. (c) Layout of the stacked SRRs

Firstly, the effective permeability of the stacked SRRs is simulated using the method proposed by Smith et al (Smith et al, 2005). The simulation results are shown in Fig. 20. It is seen that the peak value increases with the number of SRR layer, and a stabilization is achieved when there are more than four SRR layers. Then, in what follows, the microwave sensor based on stacked SRRs with four layers is discussed in detail.

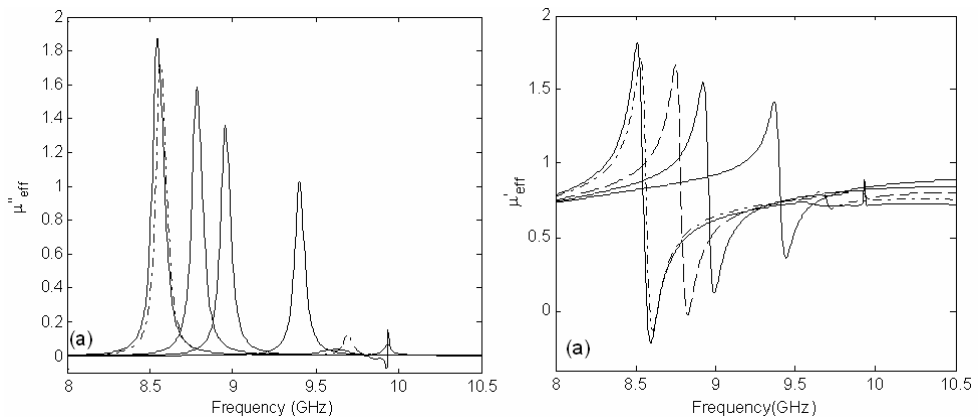


Fig. 20. Effective permeability of the stacked SRRs. (a) Real part. (b) Imaginary part. From right to left, the curves correspond to the simulation results of the stacked SRRs with one layer, two, three, four and five layers

Fig. 21 shows the electric field distribution in the vicinity of the SRR cells. It is seen that the strongest field amplitude is located in the upper slits of the SRRs, so that these areas become very sensitive to changes in the dielectric environment. Since the electric field distributions in the slits of the second and the third SRRs are much stronger than the others, to further

investigate the potential application of the stacked SRRs in dielectric sensing, thickness of the SRRs is increased to 0.1mm, and testing samples are located in upper slits the second and the third SRRs. Simulation results of transmission coefficients for a variation of sample permittivity are shown in Fig. 22.

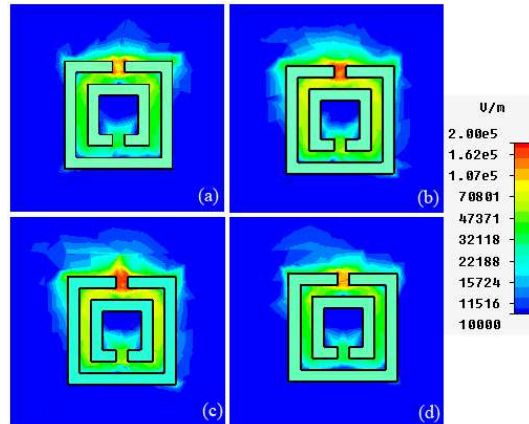


Fig. 21. Electric field distribution in the vicinity of the four SRRs. (a) The first SRR layer ($x=-0.734$ mm). (b) The second SRR layer ($x=0.515$ mm). (c) The third SRR layer ($x=1.765$ mm). (d) The fourth SRR layer ($x=3.014$ mm)

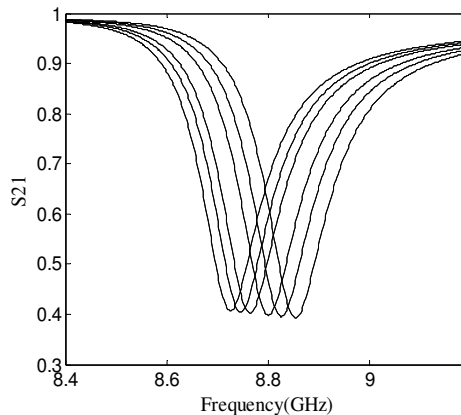


Fig. 22. Transmission coefficient as a function of frequency for a variation of sample permittivity. From right to the left, the curves are corresponding to dielectric sample with permittivity of 1, 1.5, 2, 2.5, 3 and 3.5, respectively

In conclusion, when the stacked SRRs are located in the waveguide, sample permittivity varies linearly with the frequency shift of the transmission coefficient. Although the periodic structures of SRRs (Lee et al, 2006; Melik et al, 2009; Papisimakis et al, 2010) have been used for biosensing and telemetric sensing of surface strains, etc. The above simulation results demonstrate that the stacked SRRs can also be used in dielectric sensing.

6. Open resonator using metamaterials

6.1 Open microwave resonator

For the model shown in Fig. 23, suppose the incident electric field is polarized perpendicular to the plane of incidence, that is, $\vec{E}^{(i)} = E^{(i)}\vec{e}_y$, then the incident, reflected, and refracted (transmitted) field can be obtained as

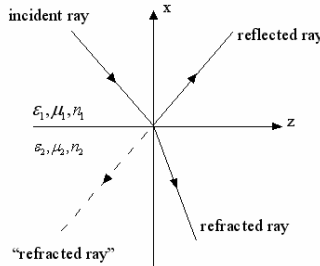


Fig. 23. Snell's law for $n_1 > 0$ and $n_2 > 0$ (real line). The dashed line for $n_1 > 0$ and $n_2 < 0$

$$\frac{E_0^{(t)}}{E_0^{(i)}} = \frac{2n_1 \cos \phi_1 / \mu_1}{n_1 \cos \phi_1 / \mu_1 + n_2(1 - n_1^2 \sin^2 \phi_1 / n_2^2)^{1/2} / \mu_2} \tag{25}$$

$$\frac{E_0^{(r)}}{E_0^{(i)}} = \frac{n_1 \cos \phi_1 / \mu_1 - n_2(1 - n_1^2 \sin^2 \phi_1 / n_2^2)^{1/2} / \mu_2}{n_1 \cos \phi_1 / \mu_1 + n_2(1 - n_1^2 \sin^2 \phi_1 / n_2^2)^{1/2} / \mu_2} \tag{26}$$

where $E_0^{(t)}$, $E_0^{(r)}$ and $E_0^{(i)}$ are the amplitudes of the transmitted, reflected, and the incident electric fields, respectively. Provided that $(n_1^2 / n_2^2) \sin^2 \phi_1 < 1$, the above formulas are valid for positive as well as negative index media. For $(n_1^2 / n_2^2) \sin^2 \phi_1 > 1$, the expression

$$(1 - n_1^2 \sin^2 \phi_1 / n_2^2)^{1/2} = \pm j(n_1^2 \sin^2 \phi_1 / n_2^2 - 1)^{1/2} . \tag{27}$$

The $-$ sign is chosen because the transmitted field must not diverge at infinity for $n_2 > 0$. The $+$ sign is chosen for $n_2 < 0$. If $n_1 > 0$ and $n_2 < 0$ and if $\epsilon_2 = -\epsilon_1$ and $\mu_2 = -\mu_1$, then $E_0^r = 0$. This means that there is no reflected field. Some interesting scenario shown in Fig. 24 can be envisioned. Fig. 24(a) illustrates the mirror-inverted imaging effect. Due to the exist of many closed optical paths running across the four interfaces, an open cavity is formed as shown in Fig. 24(b), although there is no reflecting wall surrounding the cavity.

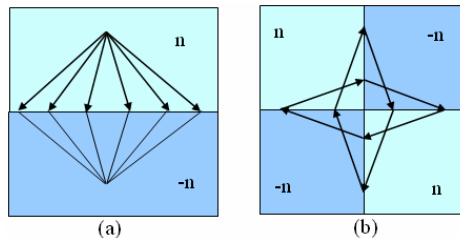


Fig. 24. (a)Mirror-inverted imaging effect. (b) Formation of an open cavity

As shown in Fig. 25(a), the open microwave resonator consists of two homogenous metamaterial squares in air. Its resonating modes are calculated using eigenfrequency model of the software COMSOL. Fig.25 (b) shows the mode around the frequency of 260MHz. It is in agreement with the even mode reported by He et al. (He et al, 2005). In the simulation, scattering boundary condition is added to the outer boundary to model the open resonating cavity. From Fig. 25(b), it is seen that electric field distribution is confined to the tip point of the two metamaterial squares. Therefore, it will be very sensitive in dielectric environment. The dependence of resonant frequency on the permittivity of dielectric environment is shown in Table 2. It is seen that when the permittivity changes from 1 to $1+10^{-8}$, the variation of resonant frequency is about 14KHz. The variation of resonant frequency can be easily detected using traditional measuring technique. Therefore, the open cavity based on metamaterials possesses high sensitivity, and it has potential application for biosensors.

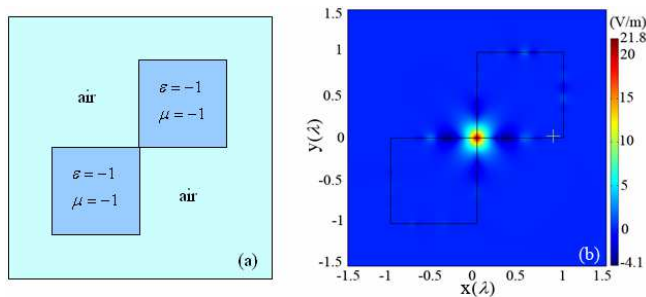


Fig. 25. (a) A subwavelength open resonator consisting of two homogenous metamaterial squares in air. (b) The electric field (E_z) distribution for (a)

Frequency(MHz)	260.481	260.467	260.336	259.794	255.372	240.485
Permittivity	1	$1+10^{-8}$	$1+10^{-7}$	$1+5 \times 10^{-7}$	$1+10^{-6}$	$1+5 \times 10^{-6}$

Table 2. The relation between resonant frequency and environment permittivity

The open resonator using metamaterials was first suggested and analyzed by Notomi (Notomi, 2000), which is based on the ray theory. Later, He et al. used the FDTD to calculate resonating modes of the open cavity.

6.2 Microcavity resonator

Fig. 26(a) shows a typical geometry of a microcavity ring resonator (Hagness et al, 1997). The two tangential straight waveguides serve as evanescent wave input and output couplers. The coupling efficiency between the waveguides and the ring is controlled by the size, g , of the air gap, the surrounding medium and the ring outer diameter, d , which affects the coupling interaction length. The width of WG1, WG2 and microring waveguide is $0.3 \mu\text{m}$. The straight waveguide support only one symmetric and one antisymmetric mode at $\lambda = 1.5 \mu\text{m}$. Fig. 26(b) is the geometry of the microcavity ring when a layer of metamaterials (the grey region) is added to the outside of the ring. The refractive index of the metamaterials is $n=-1$.

Fig. 27 is the visualization of snapshots in time of the FDTD computed field as the pulse first ($t=10\text{fs}$) couples into the microring cavity and completes one round trip ($t=220\text{fs}$). When refractive index of the surrounding medium varies from 1 to 1.3, the spectra are calculated,

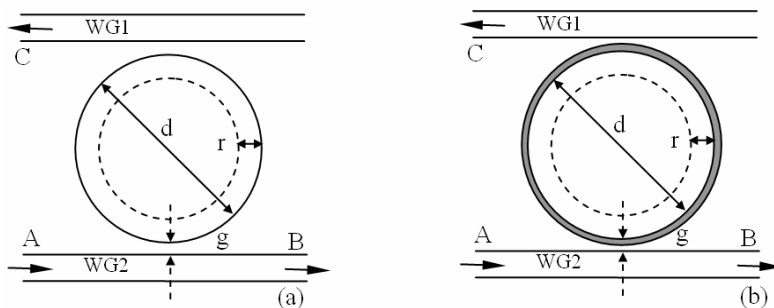


Fig. 26. (a) The schematic of a microcavity ring resonator coupled to two straight waveguides. (b) A metamaterial ring (the grey region) is added to the out side of the microring. $d=5.0\mu\text{m}$, $g=0.23\mu\text{m}$, $r=0.3\mu\text{m}$, the thickness of the metamaterials is $r/3$

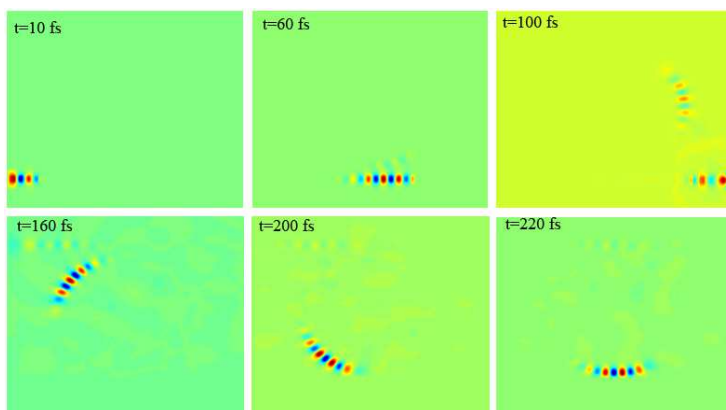


Fig. 27. Visualization of the initial coupling and circulation of the exciting pulse around the microring cavity resonators

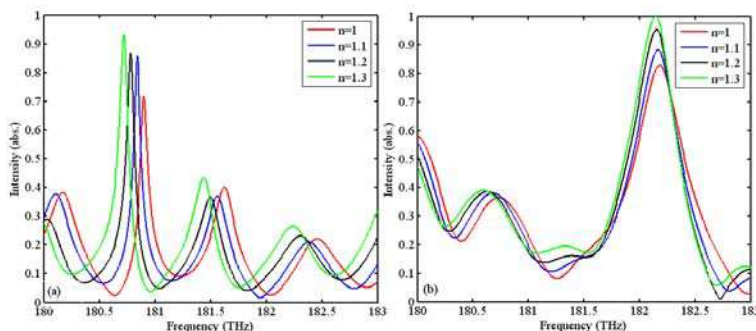


Fig. 28. Spectra for the surrounding medium with different refractive index. (a) Results for the microring cavity without metamaterial layer. (b) Results for the microring cavity with metamaterial layer

as shown in Fig. 28. From Fig. 28(a), it is seen that the resonance peak of the microring cavity without metamaterial layer is highly dependent on the refractive index of the surrounding medium, and it is red shifted with the increase of refractive index. From Fig. 28(b) we can clearly observe that the resonance peaks are shifted to the high frequency side when metamaterial layer is added to the outside of the microring ring resonator. Meanwhile, the peak value increases with the increase of the refractive index of surrounding medium. Due to its characteristics of high Q factor, wide free spectral-range, microcavity can be used in the field of identification and monitoring of proteins, DNA, peptides, toxin molecules, and nanoparticle, etc. It has attracted extensive attention world wide, and more details about microcavity can be found in the original work of Quan and Zhu et al (Quan et al, 2005; Zhu et al, 2009).

7. Conclusion

It has been demonstrated that the evanescent wave can be amplified by the metamaterials. This unique property is helpful for enhancing the sensitivity of sensor, and can realize subwavelength resolution of image and detection beyond diffraction limit. Enhancement of sensitivity in slab waveguide with TM mode is proved analytically. The phenomenon of evanescent wave amplification is confirmed in slab waveguide and slab lens. The perfect imaging properties of planar lens was proved by transmission optics. Microwave sensors based on the waveguide filled with metamaterial particles are simulated, and their sensitivity is much higher than traditional microwave sensor. The open microwave resonator consists of two homogenous metamaterial squares is very sensitive to dielectric environment. The microcavity ring resonator with metamaterial layer possesses some new properties.

Metamaterials increases the designing flexibility of sensors, and dramatically improves their performance. Sensors using metamaterials may hope to fuel the revolution of sensing technology.

8. Acknowledgement

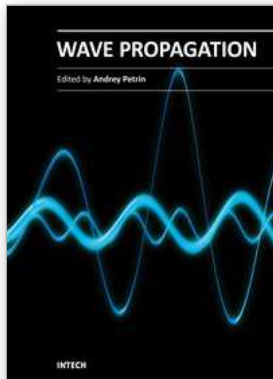
This work was supported by the National Natural Science Foundation of China (grant no. 60861002), the Research Foundation from Ministry of Education of China (grant no. 208133), and the Natural Science Foundation of Yunnan Province (grant no.2007F005M).

9. References

- Alù, A. & N. Engheta. (2008) Dielectric sensing in ϵ -near-zero narrow waveguide channels," *Phys. Rev. B*, Vol. 78, No. 4, 045102, ISSN: 1098-0121
- Al-Naib, I. A. I.; Jansen, C. & Koch, M. (2008) Thin-film sensing with planar asymmetric metamaterial resonators. *Appl. Phys. Lett.*, Vol. 93, No. 8, 083507, ISSN: 0031-9007
- Fedotov, V.A.; Rose, M.; Prosvirnin, S.L.; Papasimakis, N. & Zheludev, N. I. (2007) Sharp trapped-Mode resonances in planar metamaterials with a broken structural symmetry. *Phys. Rev. Lett.*, Vol. 99, No. 14, 147401, ISSN: 1079-7114
- Guru, B. S. & Hiziroglu, H. R. (1998). Plane wave propagation, In: *Electromagnetic Field Theory Fundamentals*, Guru, B. S. & Hiziroglu, H. R. (Ed.), 305-360, Cambridge University Press, ISBN: 7-111-10622-9, Cambridge, UK, New York

- Huang, M.; Yang, J. J.; Wang, J. Q. & Peng, J. H. (2007). Microwave sensor for measuring the properties of a liquid drop. *Meas. Sci. Technol.*, Vol. 18, No. 7, 1934–1938, ISSN: 0957-0233
- Huang, M., Yang, J.J., Sun, J., Shi, J.H. & Peng, J.H. (2009) Modelling and analysis of Ω -shaped double negative material-assisted microwave sensor. *J. Infrared Milli. Terahz. Waves*, Vol. 30, No. 11, 1131-1138, ISSN: 1866-6892
- He, S.; Jin Y.; Ruan, Z. C. & Kuang, J.G. (2005). On subwavelength and open resonators involving metamaterials of negative refraction index. *New J. Phys.*, Vol. 7, No. 210, ISSN: 1367-2630
- Hagness, S. C.; Rafizadeh, D.; Ho, S. T. & Taflove, A.(1997). FDTD microcavity simulations: design and experimental realization of waveguide-coupled single-mode ring and whispering-gallery-mode disk resonators. *Journal of lightwave Technology*, Vol. 15, No. 11, 2154-2164, ISSN: 0733-8724
- Kupfer, K. (2000). Microwave Moisture Sensor Systems and Their Applications, In: *Sensor Update*, Kupfer, K.; Kraszewski, A. & Knöchel, R, (Ed.), 343-376, WILEY-VCH, ISBN: 3-527-29821-5, Weinheim (Federal Republic of Germany)
- Kraszewski, A. W. (1991). Microwave aquametry-needs and perspectives. *IEEE Trans. Microwave Theory Tech.*, Vol. 39, No. 5, 828-835, ISSN: 0018-9480
- Lee, H. J. & Yook, J. G. (2008). Biosensing using split-ring resonators at microwave regime. *Appl. Phys. Lett.*, Vol. 92, No. 25, 254103, ISSN: 0003-6951
- Marqués, R.; Martel, J.; Mesa, F. & Medina, F. (2002). Left-Handed-Media simulation and transmission of EM waves in subwavelength split-ring-resonator-loaded metallic waveguides. *Phys. Rev. Lett.*, 89, No.18, 183901, ISSN: 0031-9007
- Melik, R.; Unal, E.; Perkgoz, N. K.; Puttlitz, C. & Demir, H. V. (2009). Metamaterial-based wireless strain sensors. *Appl. Phys. Lett.*, Vol. 95, No. 1, 011106, ISSN: 0003-6951
- Notomi, M. (2000). Theory of light propagation in strongly modulated photonic crystals: Refractionlike behavior in the vicinity of the photonic band gap. *Phys. Rev. B*, Vol.,62, No. 16, 10696-10705, ISSN: 1098-0121
- Pendry, J. B. (2000). Negative Refraction Makes a Perfect Lens. *Phys. Rev. Lett.*, Vol. 85, No. 18, 3966-3969, ISSN: 0031-9007
- Papasimakis, Ni.; Luo, Z.Q.; Shen, Z.X.; Angelis, F. D.; Fabrizio, E. D.; Nikolaenko, A. E.; & Zheludev, N. I. (2010). Graphene in a photonic metamaterial. *Optics Express*, Vol. 18, No. 8, 8353-8359, ISSN: 1094-4087
- Qing, D. K. & Chen, G. (2004). Enhancement of evanescent waves in waveguides using metamaterials of negative permittivity and permeability. *Appl. Phys. Lett.*, Vol. 84, No. 5, 669-671, ISSN: 0003-6951
- Quan, H.Y.; & Guo, Z.X. (2005). Simulation of whispering-gallery-mode resonance shifts for optical miniature biosensors. *Journal of Quantitative Spectroscopy & Radiative Transfer*, Vol. 93, No. 1-3, 231–243, ISSN: 0022-4073
- Shelby, R. A.; Smith, D. R. & Schultz, S. (2001). Experimental verification of a negative index of refraction. *Science*, Vol. 292, No. 5514, 77-79, ISSN: 0036-8075
- Service, R. F. (2010). Next wave of metamaterials hopes to fuel the revolution. *Science*, Vol. 327, No. 5962, 138-139, ISSN: 0036-8075

- Shreiber, D.; Gupta, M. & Cravey, R. (2008). Microwave nondestructive evaluation of dielectric materials with a metamaterial lens. *Sensors and Actuators*, Vol. 144, No.1, 48-55, ISSN : 0924-4247
- Silveirinha, M. & Engheta, N. (2006). Tunneling of Electromagnetic Energy through Subwavelength Channels and Bends using ϵ -Near-Zero Materials. *Phys. Rev. Lett.*, Vol. 97, No. 15, 157403, ISSN: 0031-9007
- Smith, D. R.; Vier, D C; Koschny, Th. & Soukoulis, C. M. (2005). Electromagnetic parameter retrieval from inhomogeneous metamaterials. *Phys. Rev. E*, Vol. 71, No. 3, 036617, ISSN: 1539-3755
- Taya, S. A.; Shabat, M. M. & Khalil, H. M.(2009). Enhancement of sensitivity in optical waveguide sensors using left-handed materials. *Optik*, Vol. 120, No.10, 504-508, ISSN: 0030-4026
- Von Hippel A, (1995). Dielectric measuring techniques, In: *Dielectric Materials and Applications*, Hippel A. V., (Ed.) 47-146, Wiley/The Technology Press of MIT, ISBN: 0-89006-805-4, New York
- Veselago, V. G. (1968). The electrodynamics of substances with simultaneously negative values of ϵ and μ . *Sov. Phys. Usp.*, Vol. 10, No. 4, (1968) 509-514, ISSN: 0038-5670
- Wang,W.; Lin, L.; Yang, X. F. Cui, J. H.; Du, C. L. & Luo, X. G. (2008). Design of oblate cylindrical perfect lens using coordinate transformation. *Optics Express*, Vol. 16, No. 11, 8094-8105, ISSN: 1094-4087
- Wu, Z.Y.; Huang, M.; Yang J. J.; Peng, J.H. & Zong, R. (2008). Electromagnetic wave tunnelling and squeezing effects through 3D coaxial waveguide channel filled with ENZ material, *Proceedings of ISAPE 2008*, pp. 752-755, ISBN: 978-1-4244-2192-3, Kunming, Yunnan, China, Nov. 2008, Institute of Electrical and Electronics Engineers, Inc., Beijing
- Yang J. J.; Huang, M.; Xiao, Z. & Peng, J. H.(2010). Simulation and analysis of asymmetric metamaterial resonator-assisted microwave sensor. *Mod. Phys. Lett. B*, Vol. 24, No. 12, 1207-1215, ISSN: 0217-9849
- Zoran, J.; Jakšić, O.; Djuric,Z. & Kment, C. (2007). A consideration of the use of metamaterials for sensing applications:field fluctuations and ultimate performance, *J. Opt. A: Pure Appl.*, Vol. 9, No. 9, S377-S384, ISSN: 1464-4258
- Zhu, J.G.; Ozdemir, S. K.; Xiao, Y. F.; Li, L.; He, L.N. Chen, D.R. & Yang, L.(2009). On-chip single nanoparticle detection and sizing by mode splitting in an ultrahigh-Q microresonator. *Nature Photonics*, Vol. 4, No.1, 46-49, ISSN: 1749-4885



Wave Propagation

Edited by Dr. Andrey Petrin

ISBN 978-953-307-275-3

Hard cover, 570 pages

Publisher InTech

Published online 16, March, 2011

Published in print edition March, 2011

The book collects original and innovative research studies of the experienced and actively working scientists in the field of wave propagation which produced new methods in this area of research and obtained new and important results. Every chapter of this book is the result of the authors achieved in the particular field of research. The themes of the studies vary from investigation on modern applications such as metamaterials, photonic crystals and nanofocusing of light to the traditional engineering applications of electrodynamics such as antennas, waveguides and radar investigations.

How to reference

In order to correctly reference this scholarly work, feel free to copy and paste the following:

Ming Huang and Jingjing Yang (2011). Microwave Sensor Using Metamaterials, Wave Propagation, Dr. Andrey Petrin (Ed.), ISBN: 978-953-307-275-3, InTech, Available from: <http://www.intechopen.com/books/wave-propagation/microwave-sensor-using-metamaterials>

INTECH

open science | open minds

InTech Europe

University Campus STeP Ri
Slavka Krautzeka 83/A
51000 Rijeka, Croatia
Phone: +385 (51) 770 447
Fax: +385 (51) 686 166
www.intechopen.com

InTech China

Unit 405, Office Block, Hotel Equatorial Shanghai
No.65, Yan An Road (West), Shanghai, 200040, China
中国上海市延安西路65号上海国际贵都大饭店办公楼405单元
Phone: +86-21-62489820
Fax: +86-21-62489821

© 2011 The Author(s). Licensee IntechOpen. This chapter is distributed under the terms of the [Creative Commons Attribution-NonCommercial-ShareAlike-3.0 License](#), which permits use, distribution and reproduction for non-commercial purposes, provided the original is properly cited and derivative works building on this content are distributed under the same license.